Journal of Global Environment Engineering, Vol. 8, pp. 17-33, 2002

MEASUREMENT OF OPTICAL AND CHEMICAL PROPERTIES OF ATMOSPHERIC AEROSOLS OVER THE WESTERN PACIFIC OCEAN

FUJITANI Yuji[1]
OHTA Sachio[2]
ENDOH Tatsuo[3]
MURAO Naoto[4]
YAMAGATA Sadamu[5]

Abstract

It is necessary to determine the spatial distribution and variation of optical properties and chemical species of atmospheric aerosols to estimate their direct effect on climate. In the western Pacific Ocean, where pollutants are transported from East Asia, there are few aerosol measurements available to estimate the climatic effects. In this study the optical and chemical properties of aerosols were measured on board the R/V Mirai in June-July 2000 (MR00-K04 cruise) and in May 2001 (MR01-K02 cruise) in the western Pacific Ocean during the ACE-Asia campaign.

The MR00-K04 cruise covered the maritime air mass south of 30° N. The median volume absorption coefficient (σ_{ap}) was extremely low, $1\times10^{-7}m^{-1}$, and the volume scattering coefficient (σ_{sp}) ranged from 7.0×10^{-6} to 33.7×10^{-6} m^{-1}. The single scattering albedo ($\omega=\sigma_{sp}/(\sigma_{sp}+\sigma_{ap})$), ranged from 0.97 to 0.99. During the MR01-K02 cruise, anthropogenic aerosols and soil particles emitted from Asian countries were detected at a distance of 500 km from the coast. In this area, the median σ_{ap} was 2.2×10^{-6} m^{-1}, 20 times higher than that measured south of 30° N in the MR00-K04 cruise. The ω values were 0.82 - 1.0 and the median of the aerosol optical thickness (AOT) at 550nm wavelength was 0.50 which was 8 times that on MR00-K04.

KEYWORDS: Aerosols, Optical properties, Pacific Ocean, ACE-Asia

1. Introduction

Atmospheric aerosols affect climate by perturbing the radiation budget through scattering and absorbing solar radiation, the direct effect of aerosols (Charlson et al., 1992). At present, the

1 Division of Environment and Resource Engineering, Graduate School of Engineering, Hokkaido Univ., Sapporo 060-8628, Japan
2 D.Sci., Prof., Div. of Environment and Resource Engineering, Graduate School of Engineering, Hokkaido Univ.
3 D.Sci., Associate Prof., Institute of Low Temperature Science, Hokkaido Univ.
4 D.Eng., Associate Prof., Div. of Environment and Resource Engineering, Graduate School of Engineering, Hokkaido Univ.
5 D.Eng., Instructor, Div., of Environment and Resource Engineering, Graduate School of Engineering, Hokkaido Univ.

uncertainty in radiative forcing due to greenhouse gases is 15%, while it is a factor of 2 for the direct aerosol forcing (IPCC, 1996). The larger uncertainty in aerosol forcing derives from a limited knowledge of the distribution of aerosol optical properties. There are a number of sources and sinks for aerosol, and lifetimes are as short as a week or 10 days. As a result, aerosols have various spatial distributions and temporal variations. Further, aerosol optical properties are a function of the aerosol chemical species, size distribution, and mixing state (i.e. internal mixture or external mixture). It is then necessary to conduct long term and large-area observations of optical and chemical properties of aerosols.

There are particularly few measurements of aerosol optical properties over the Pacific Ocean. Anthropogenic compounds are increasingly emitted from Asian countries, and more aerosols may be transported to the Pacific Ocean. Thus, it is important to monitor atmospheric aerosols in East Asia and the western Pacific Ocean. Satellite remote sensing is hoped to be able to monitor the global aerosol distribution (Nakajima et al., 1999), but for atmospheric correction or retrieving the aerosol optical thickness of the remote sensing, surface measurements are indispensable to establish the optical properties, in particular the single scattering albedo ω and the chemical properties of atmospheric aerosols.

Various field studies have been conducted, and especially the Aerosol Characterization Experiment (ACE) is on a large scale, it is a co-operative project organized by the International Global Atmospheric Chemistry (IGAC). The ACE-1 survey was conducted in the Southern Ocean near Tasmania, a remote marine region in 1995; ACE-2 was carried out over the North Atlantic Ocean in 1997 to investigate characteristics of anthropogenic aerosols from the European continent and from the Sahara desert; ACE-Asia is planed for 2000 to 2004 to determine the optical and chemical properties of aerosols and to evaluate their effect on climate in the East Asia and Northwest Pacific regions.

This paper reports results of aerosol measurements on board R/V Mirai over the Pacific Ocean in 2000 and 2001 during pre-ACE-Asia and ACE-Asia.

2. Methods of Measurement and Analysis

2.1 Obeservation

The authors participated in the MR00-K04 cruise of R/V Mirai (Japan Marine Science and Technology Center) from June 13 to July 6, 2000 as shown in Fig. 1. The R/V Mirai departed from Sekinehama, Aomori prefecture, on June 13 and cruised southwards along the 140° E longitude from 30° N to 5° N. From June 20 to June 30, observation was conducted while stationary at 7° N, 140° E. Then R/V Mirai departed from the stationary observation point on July 1 and cruised northward to Yokosuka, Kanagawa prefecture. Overall measurements were conducted from 18:00 June 13 to 16:00 July 5.

We also joined the MR01-K02 cruise of R/V Mirai on May 14 - 28, 2001 as shown in Fig. 2. It departed from Yokosuka on May 14 sailed east to 152° E and cruised northward on 17 - 27 May from 30° N to 40° N along the 146° E longitude and entered Sekinehama on May 28; measurements had been conducted from 9:00 May 14 to 3:00 July 28.

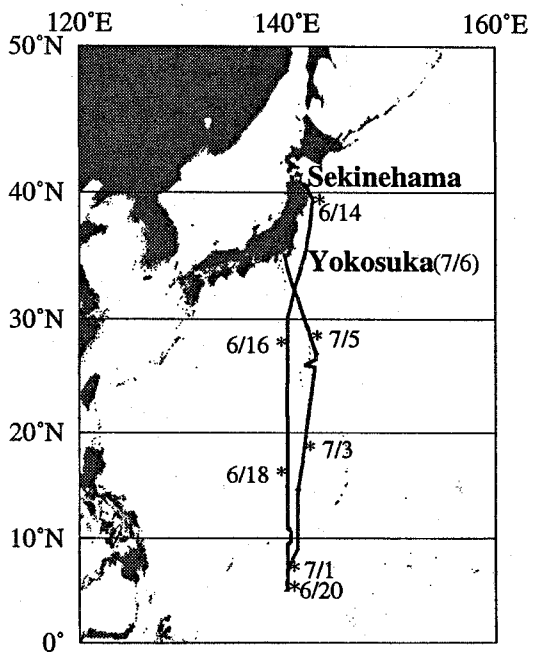

Figure 1. The MR00-K04 cruise (Jun. 13 -Jul. 6, 2000).

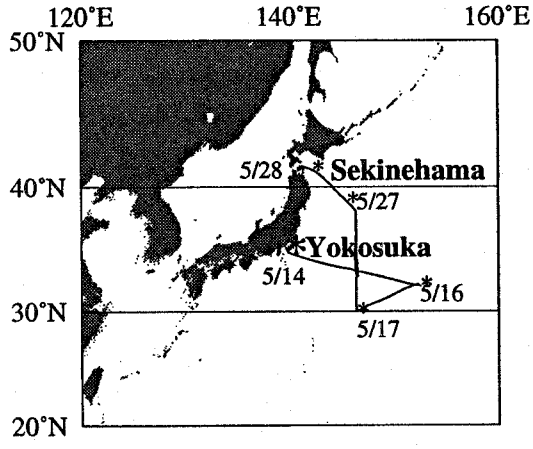

Figure 2. The MR01-K02 cruise (May 14 - 28, 2001).

2.2 Measurements

Sample air was drawn at a flow rate of 20 L min^{-1} through inlets at a height of 27m above sea level. Air passed through a 10mm internal diameter tube, 26m long from inlet to the manifold in the research room. To remove coarse particles, a cyclone separator with 50 percent cut-off particle diameter (D_P) of 2.0 μm was attached. From the manifold, sample air was distributed to a Particle Soot/ Absorption Photometer (PSAP, Radiance Research), an Integrating Nephelometer (IN, M903, Radiance Research), and an Optical Particle Counter (OPC, KC-01C, Rion). All measurements were recorded every minute. The IN measured the volume scattering coefficient (σ_{sp}) at wavelength 530nm. The calibration was carried out by using particle free air and pure CO_2. The OPC counts the number concentration of aerosols larger than 0.3, 0.5, 1.0, 2.0, and 5.0 μm diameter. The PSAP measured the volume absorption coefficient (σ_{ap}) using the Integrating Plate Method. The light at 565nm wavelength rays on a filter (Pallflex Membrane Filter, Gelman Sciences) and monitors the change in transmission thorough the filter. In a remote area as the Pacific Ocean, the transmissions are not sensible at 1 minute intervals, then we calculated σ_{ap} by equation (1),

$$\sigma_{ap} = \frac{A}{V} \ln\left[\frac{\tau_0}{\tau}\right] \times f \qquad (1)$$

where V is the sampled air volume [m^3] and A is the sampling spot area [m^2]. In this study, we used $A=1.968\times10^{-5}$ m^{-2} instead of the value in the manual. The τ_0 and τ are the first and last values of transmission in the interval. The f value is a correction factor for overestimates of σ_{ap} proper in the Integrating Plate Method, which is derived as follows (Bond et al., 1999);

$$f = \frac{1}{2(0.5398 \times \tau + 0.355)} \qquad (2)$$

For removing the contamination from ship exhaust, we removed values of τ when the relative wind direction was between 90 and 270 degrees from the ship head or when the relative wind speed was below 1m sec^{-1}, and when the ship had stopped. Though the particle number suddenly increased when sample air caught the ship exhaust, no sudden increase as found when the relative wind direction was ± 90 degree from the ship head and the relative wind speed was over 1m sec^{-1}.

After the contaminated values of τ from the ship exhaust were removed, we used the first and the last τ in each successive dataset (1-15 hours) to calculate σ_{ap} in Eqs. (1) and (2). The detection limit of σ_{ap} is $1.0 \times 10^{-7} m^{-1}$ at 1 hour, which was estimated from the measurements of the drift of the signal setting in the filter blank. As for the values of σ_{sp}, we calculated the 10min average after removing values contaminated by the ship exhaust. We determined ω by using σ_{ap} and the arithmetic mean σ_{sp} during the same period as that for the σ_{ap} calculation.

Aerosols were also collected on filters for chemical analysis by two sampling systems. One is a Teflon filter (FP-500; 47mm ϕ; Sumitomo electric) sampling line, and the other is a quartz fiber filter (2500QAT-UP; 47mm ϕ; Pallflex) sampling line. Both sampling lines also used the cyclone separators to remove coarse particles ($D_P > 2\mu m$). The filter samplings were performed while ensuring that there was no contamination by chimney exhaust (i.e., the samplings was stopped when the wind direction was from the chimney or the ship had stopped). After finishing sampling, the filters were covered with aluminum foil and stored in a refrigerator. Tables 1 and 2 show results of the filter sampling in MR00-K04 and MR01-K02, respectively. Aerosol collected on Teflon filters had the ionic components extracted in ion exchanged distilled water and analyzed by ion chromatography (DX500, Dionex). The metal components were extracted from the Teflon filters in a solution of nitric and hydrofluoric acids, and then analyzed by an induced coupled plasma mass spectrometer (ICP-MS, HP4500, Hewlett Packard). The aerosol collected on quartz fiber filters were treated by heating in air at 300℃ for 30 minutes to remove organic carbon. From the treated quartz fiber filters the amounts of elemental carbon (EC) were determined by a carbon analyzer (Ohta and Okita, 1984).

We analyzed the ionic components of Na^+, NH_4^+, K^+, Mg^{2+}, Ca^{2+}, Cl^-, NO_3^-, and SO_4^{2-}. The amount of non-sea salt sulfate (NSS-SO_4^{2-}) was determined by assuming that the concentration of SO_4^{2-} derived from seawater is equal to 0.251 times the Na^+ concentration, and then subtracting that from the total SO_4^{2-}. The analyzed metal components were Mg, Al, V, Cr, Mn, Fe, Ni, Cu, Zn, As, Cd, and Pb. The amount of non-crustal metal component X (NC-X) was determined as the amount of X in the earth crust, which was calculated from the Al to X ratio in the crust and deducted from the total amount of X in the aerosol sample. The detection limit of the concentration was set as twice the filter blank.

A sky-radiometer (POM-01MK Ⅱ, PREDE) measured the direct and aureole of the sunlight at wavelengths 400, 500, 675, 870, and 1020nm. From these data, it is possible to retrieve the aerosol optical thickness and aerosol size distribution (Nakajima et al., 1996).

Table 1. Information of aerosol sampling on Teflon and quartz fiber filters in the MR00-K04 cruise. JST Japan Standard Time.

Teflon filter							Quartz fiber filter						
No.	Date and time (JST)		Sampling volume [m³]	Latitude (deg)			No.	Date and time (JST)		Sampling volume [m³]	Latitude (deg)		
	Start	End		Start	End			Start	End		Start	End	
0004T02	13Jun. 17:46	14Jun. 8:01	17.4	40.6	37.1		0004Q02	13Jun. 17:46	14Jun. 8:01	17.0	40.6	37.1	
0004T03	14Jun. 8:50	15Jun. 8:16	28.1	36.9	31.6		0004Q04	14Jun. 8:50	15Jun. 8:16	28.4	36.9	31.6	
0004T04	15Jun. 8:50	16Jun. 8:44	27.6	31.5	25.6		0004Q05	15Jun. 8:50	16Jun. 8:44	28.0	31.5	25.6	
0004T05	16Jun. 9:54	17Jun. 18:44	34.1	25.3	17.5	Southbound period	0004Q06	16Jun. 9:54	18Jun. 4:21	45.4	25.3	15.0	
0004T06	17Jun. 19:06	19Jun. 10:50	37.6	17.3	8.4		0004Q07	18Jun. 8:24	20Jun. 8:54	53.3	14.7	6.7	
0004T07	19Jun. 11:11	20Jun. 8:54	25.6	8.3	6.7								
0004T08	20Jun. 9:22	21Jun. 23:10	33.3				0004Q08	20Jun. 9:22	21Jun. 23:10	32.9			
0004T09	21Jun. 23:56	23Jun. 16:42	34.4				0004Q09	21Jun. 23:56	24Jun. 13:41	52.3			
0004T10	23Jun. 17:44	25Jun. 11:11	36.4	7.0		Stationary obeservation period	0004Q10	24Jun. 14:34	26Jun. 19:04	42.7	7.0		
0004T11	25Jun. 12:46	26Jun. 19:04	25.2										
0004T12	26Jun. 21:05	28Jun. 16:18	29.7				0004Q11	26Jun. 21:05	29Jun. 22:29	50.3			
0004T13	28Jun. 17:52	29Jun. 22:29	20.0										
0004T14	29Jun. 23:44	1Jul. 11:53	29.0	7.0	9.7		0004Q12	29Jun. 23:44	2Jul. 12:28	54.7	7.0	15.5	
0004T15	1Jul. 14:42	2Jul. 12:28	25.2	10.4	15.5								
0004T16	2Jul. 14:51	3Jul. 14:42	28.6	16.1	21.8	Northbound period	0004Q13	2Jul. 14:51	4Jul. 17:34	56.8	16.1	26.9	
0004T17	3Jul. 15:02	4Jul. 17:34	27.2	21.9	26.9								
0004T18	4Jul. 17:57	5Jul. 13:49	23.7	27.0	31.5		0004Q14	4Jul. 17:57	5Jul. 13:49	24.2	27.0	31.5	

Table 2. Same as Table 1 but for the MR01-K02 cruise.

Teflon filter								Quartz fiber filter							
No.	Date and time (JST)		Sampling volume [m³]	Start (deg)		End (deg)		No.	Date and time (JST)		Sampling volume [m³]	Start (deg)		End (deg)	
	Start	End		Latitude	Longtitude	Latitude	Longtitude		Start	End		Latitude	Longtitude	Latitude	Longtitude
0102T01	14May. 8:55	14May. 15:45	8.2	35.3	139.7	34.5	141.2	0102Q01	14May. 8:55	14May. 15:45	8.2	35.3	139.7	34.5	141.2
0102T02	14May. 16:36	15May. 8:00	18.5	34.4	141.5	33.3	146.5	0102Q02	14May. 16:36	15May. 8:00	18.5	34.4	141.5	33.3	146.5
0102T03	15May. 8:31	16May. 4:32	23.6	33.3	146.6	32.2	152.4	0102Q03	15May. 8:31	16May. 4:32	23.6	33.3	146.6	32.2	152.4
0102T04	16May. 8:26	17May. 19:00	19.7	32.1	152.5	30.2	146.4	0102Q04	16May. 8:26	18May. 10:41	19.2	32.1	152.5	30.8	146.4
0102T05	17May. 19:15	18May. 20:12	28.5	30.2	146.4	31.3	146.4								
0102T06	18May. 20:17	20May. 10:41	29.1	31.3	146.4	33.3	146.4	0102Q05	18May. 10:55	20May. 20:32	21.0	30.8	146.4	33.5	146.4
0102T07	20May. 10:45	21May. 20:35	26.9	33.3	146.4	33.8	146.5								
0102T08	21May. 20:40	23May. 15:56	23.8	33.8	146.5	35.4	146.4	0102Q06	21May. 5:55	23May. 15:56	40.0	33.1	146.4	35.4	146.4
0102T09	23May. 16:35	24May. 20:38	30.4	35.4	146.3	34.3	146.4	0102Q07	23May. 16:35	25May. 18:40	47.6	35.4	146.3	35.2	146.4
0102T10	24May. 20:50	25May. 18:40	17.2	34.3	146.4	35.2	146.4								
0102T11	25May. 19:00	26May. 18:53	20.5	35.2	146.4	36.5	146.4	0102Q08	25May. 19:00	27May. 8:06	34.0	35.2	146.4	38.0	146.4
0102T12	26May. 18:56	27May. 8:06	13.5	36.5	146.4	38.0	146.4								
0102T13	27May. 8:30	28May. 4:48	24.3	38.0	146.4	41.2	142.2	0102Q09	27May. 8:30	28May. 4:48	24.3	38.0	146.4	41.2	142.2

Aerosol loss within the sampling system was determined by another optical particle counter (227B; Met One) at the inlet of the sampling tube, simultaneously. This OPC measured particle number concentrations larger than D_P= 0.3 and 0.5 μ m. We performed the tests three times with periods of measurements of 60min, 80min, and 100min. It was found that the particle number concentration (0.3<D_P<0.5 μ m) inside the manifold was less than 70% of that at the inlet, and the number concentration larger than 0.5 μ m in diameter was less than 45%. The data of temperature, relative humidity, wind direction, wind speed, and precipitation measured by the meteorological observation system in R/V Mirai was used. The meteorological data were averaged and recorded every 6 seconds and every 10 minutes. Backward trajectory analysis was conducted by a three-dimensional isentropic model using the global meteorological data supported by the Japan meteorological business support center. The trajectories were calculated at 925 hPa for 5 days retrospectively.

3. Results and Discussion

3.1 MR00-K04 Cruise

3.1.1 Weather Conditions

During the R/V Mirai cruise southward from 40° N (18:00 June 13) to 30° N (16:00 June 15), it rained due to the rainy season around Japan as shown in Fig. 3 which is a time series of the precipitation. After June 16, the weather was fine except for occasional squalls. North of 30° N, the wind was sometimes northerly, while south of 26° N there were easterly trade winds. South of 25° N, relative humidity and temperature were constant at 80% and 28℃, which means that the area was covered with a tropical maritime air mass.

3.1.2 Optical Properties

Figure 4 is a time series of the volume scattering coefficient (σ_{sp}), volume absorption coefficient

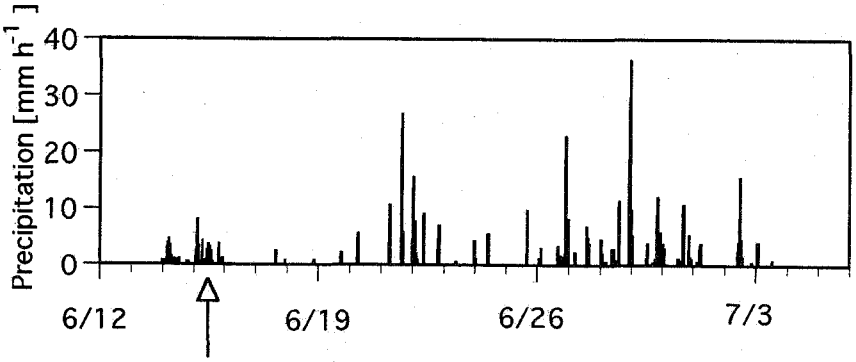

Figure 3. Time series of precipitation during the MR00-K04 cruise (Jun. 13 -Jul. 4, 2000). The arrow shows when the Mirai crossed the 30° N latitude from north to south (16:00 Jun. 15).

(σ_{ap}), single scattering albedo (ω), and aerosol optical thickness (AOT) at 550nm wavelength. And Table 3 shows the median, the lower quartile point (25%), and the upper quartile point (75%) of σ_{sp}, σ_{ap}, ω, AOT, and the angstrom exponent (α). The optical properties and chemical components

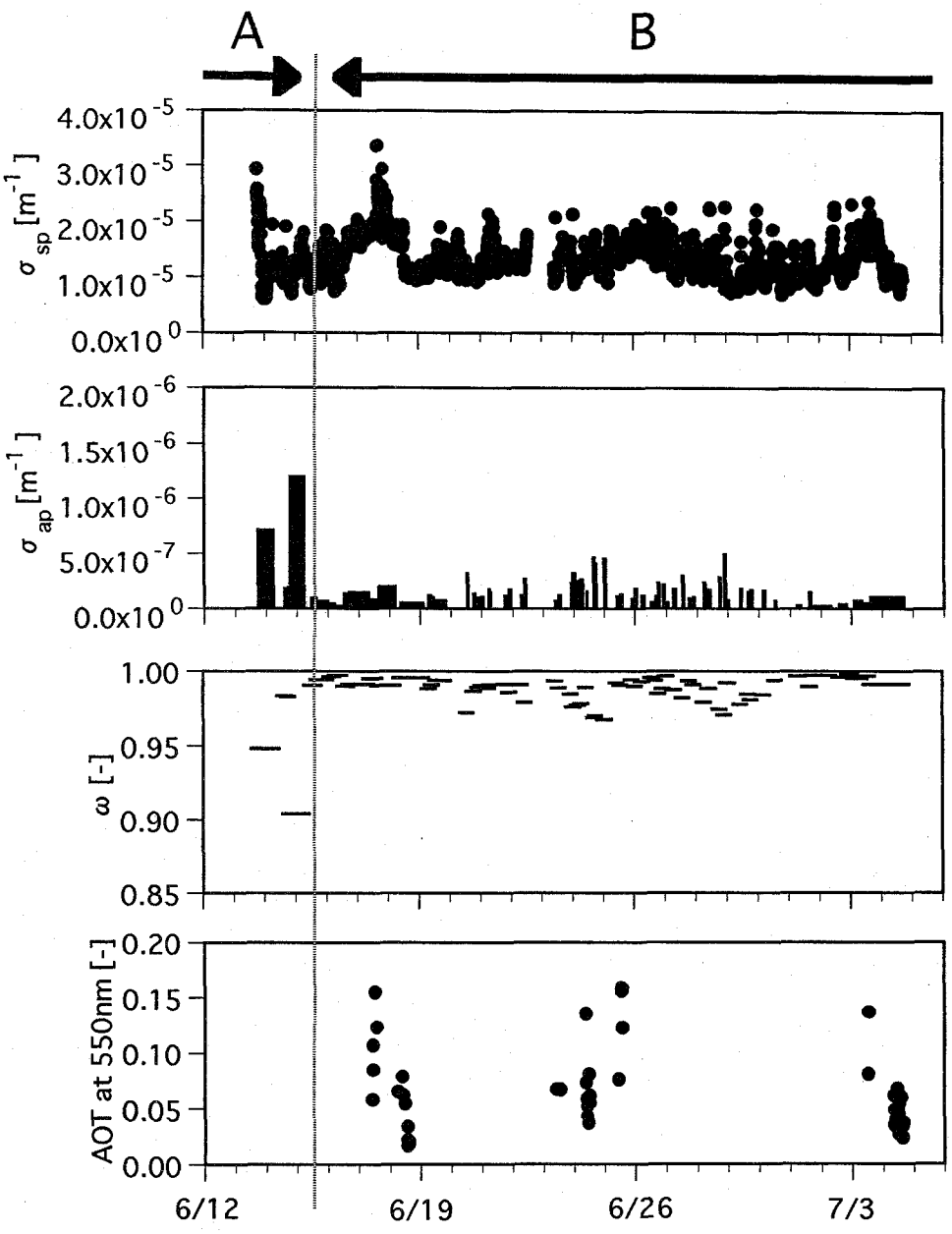

Figure 4. Time series of the volume scattering coefficient (σ_{sp}), the volume absorption coefficient (σ_{ap}), the single scattering albedo (ω), and the aerosol optical thickness (AOT) at 550nm wavelength from the MR00-K04 cruise (Jun. 13 - Jul. 4, 2000). Period A was north of 30° N (18:00 Jun. 13 to 15:00 Jun. 15), and period B south of 30° N (16:00 Jun. 15 to 17:00 Jul. 4).

Table 3. Statistics of the scattering coefficients(σ_{sp}), absorption coefficients (σ_{ap}), single scattering albedo (ω), aerosol optical thickness (AOT) at 550nm wavelength, and angstrom exponent (α) of the median, lower quartile point (25%), and upper quartile point (75%) for each period. Period A for the MR00-K04 cruise is north of 30° N (18:00 Jun. 13 to 15:00 Jun. 15, 2000), and period B south 30° N (16:00 Jun. 15 to 17:00 Jul. 4, 2000). In the MR01-K02 cruise, period C is 2:00 May 18 to 2:00 May 23, 2001, and period D 22:00 May 24 to 8:00 May 27, 2001, and period P corresponds to 18:00 May 16 to 8:00 May 17 and 3:00 May 23 to 20:00 May 24, 2001.

		MR00K04		MR01K02		
		period A	period B	period C	period D	period P
σ_{sp} [$\times 10^{-6}$ m^{-1}]	25%	9.8	10.7	9.9	12.3	4.9
	median	11.2	12.8	12.4	15.7	8.5
	75%	12.7	15.5	14.0	37.0	11.4
σ_{ap} [$\times 10^{-6}$ m^{-1}]	25%	0.31	0.05	1.88	0.86	0.07
	median	0.71	0.11	2.17	1.21	0.14
	75%	1.20	0.15	2.36	3.32	0.26
ω	25%	0.90	0.99	0.84	0.90	0.97
	median	0.95	0.99	0.85	0.92	0.98
	75%	0.98	1.00	0.86	0.94	0.99
AOT at 550nm	25%	-	0.04	0.17	0.44	-
	median	-	0.06	0.22	0.50	-
	75%	-	0.08	0.24	0.54	-
α	25%	-	0.37	0.67	0.65	-
	median	-	0.57	0.84	0.73	-
	75%	-	0.85	0.90	0.79	-

south and north of 30° N are discussed separately. The measured results north of 30° N correspond to period A (18:00 June 13 to 15:00 June 15) and south of 30° N to period B (16:00 June 15 to 17:00 July 4).

In Fig. 4, σ_{sp} and σ_{ap} had no large variations during period B. As shown in Table 3, the median value of σ_{sp} in period B was 12.8×10^{-6} m^{-1} which is a little higher than in period A. The median of σ_{ap} in period A was 7 times higher that of period B. Thus, ω ranged from 0.90 to 0.99 in period A. While in period B, ω ranged from 0.99 of the lower quartile point to 1.00 of the upper quartile point. That is, 50% of the measured ω were within 0.99 to 1.00, and light extinction occured almost only by scattering in period B. The AOT ranged from 0.02 to 0.16, and the median was 0.06 in period B. The median of α was 0.6 in period B, which means that coarse particles such as sea salt are dominant.

There are some data available for comparison with our measurement. Bodhaine (1995) reported optical properties of aerosols measured at Mauna Loa, Hawaii as representative of the mid-troposphere in the Pacific Ocean. The mean values in June and July was 1.0×10^{-6} m^{-1} for σ_{sp}, 0.4×10^{-7} m^{-1} for σ_{ap}, and 0.96 for ω. Anderson et al. (1999) measured σ_{sp} and σ_{ap} at the pacific coastal station at Cheeka Peak, Washington in spring, separating the air mass by backward trajectory analysis between Marine events and Asian-Modified Marine events. During the Marine event mean values of σ_{sp} and σ_{ap} were 3.34×10^{-6} m^{-1} and 0.9×10^{-7} m^{-1}, respectively, and the averaged ω

was 0.974. Our measured values of σ_{ap} in period B is comparable to that in the Mauna Loa and Cheeka Peak, whereas σ_{sp} is higher.

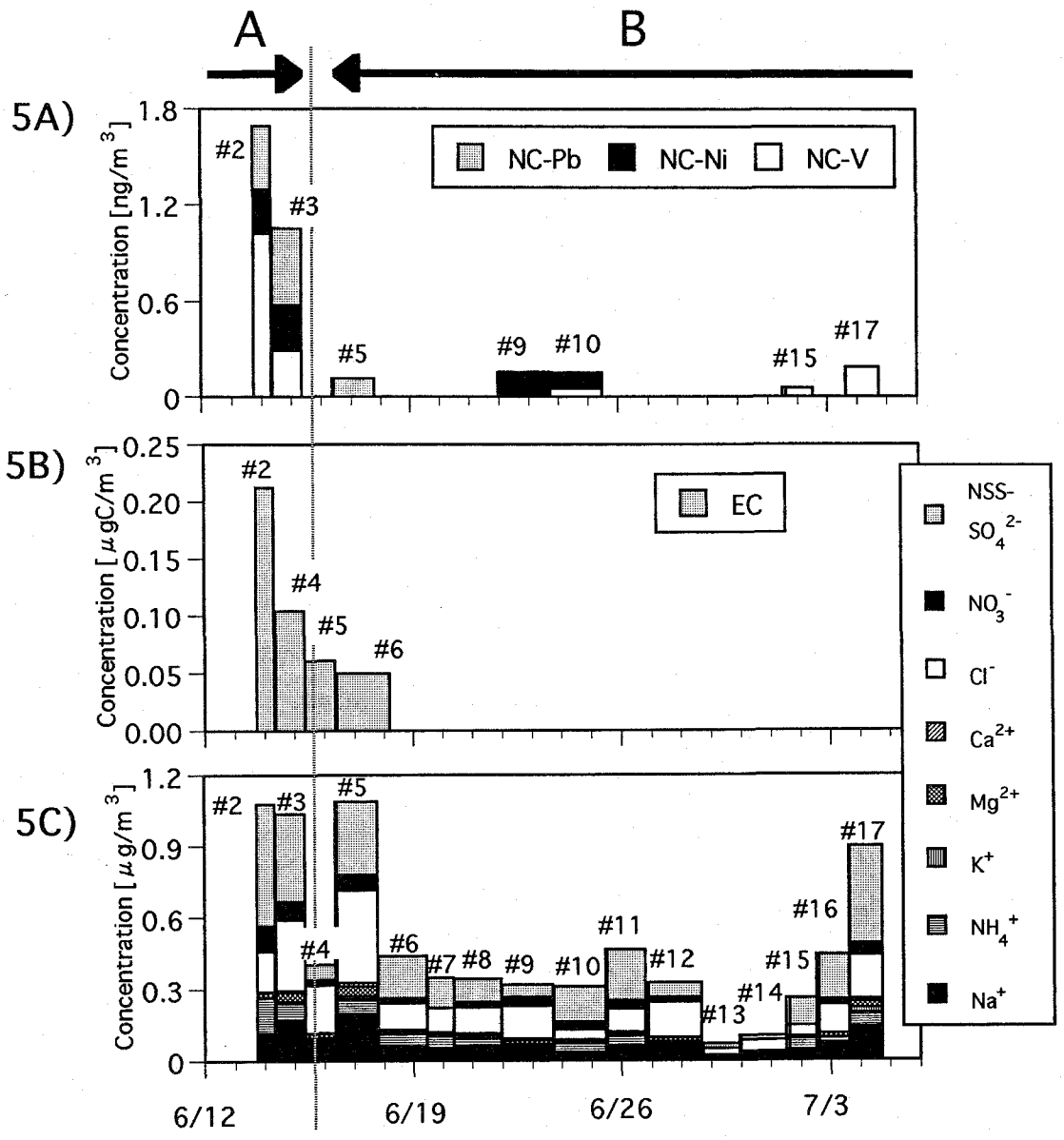

Figure 5. Time series of metal components (Fig. 5A), elemental carbon (Fig. 5B), and ionic components (Fig. 5C) in the MR00-K04 cruise (Jun. 13 -Jul. 4, 2000). #2 - #17 represent filter sample numbers. #2 - #17 in Fig. 5A and 5C, and #2 - #6 in Fig. 5B correspond to filter numbers 0004T** and 0004Q** in Tables 1 and 4.

Table 4. Concentrations of ionic components, metal components, and elemental carbon for the MR00-K04 cruise (Jun. 13 -Jul. 5, 2000). N.D. below detection limit. Units are different for different components and shown at the bottom of the table.

No.	Na^+	NH_4^+	K^+	Mg^{2+}	Ca^{2+}	Cl^-	NO_3^-	$NSS\text{-}SO_4^{2-}$	Al	Fe	NC-V	NC-Cr	NC-Ni	NC-Cu	NC-Zn	NC-As	NC-Cd	NC-Pb	No.	EC
0004T02	0.12	0.15	N.D.	0.03	N.D.	0.17	0.11	0.51	N.D.	N.D.	1.0	N.D.	0.3	4.5	N.D.	N.D.	N.D.	0.4	0004Q02	0.21
0004T03	0.17	0.07	0.01	0.04	0.01	0.30	0.08	0.37	N.D.	N.D.	0.3	N.D.	0.3	2.5	N.D.	N.D.	N.D.	0.5	0004Q04	0.10
0004T04	0.10	N.D.	N.D.	0.02	N.D.	0.20	0.02	0.06	N.D.	N.D.	N.D.	N.D.	N.D.	1.9	N.D.	N.D.	N.D.	N.D.	0004Q05	0.06
0004T05	0.20	0.06	0.01	0.04	0.02	0.39	0.06	0.31	N.D.	N.D.	N.D.	N.D.	N.D.	2.4	N.D.	N.D.	N.D.	0.1	0004Q06	0.05
0004T06	0.08	0.05	N.D.	0.01	0.01	0.11	0.02	0.18	N.D.	N.D.	N.D.	N.D.	N.D.	2.4	N.D.	N.D.	N.D.	N.D.	0004Q07	N.D.
0004T07	0.05	0.05	N.D.	0.01	0.01	0.10	N.D.	0.13	N.D.	N.D.	N.D.	N.D.	N.D.	N.D.	N.D.	N.D.	N.D.	N.D.	0004Q08	N.D.
0004T08	0.06	0.03	N.D.	0.01	0.01	0.11	0.02	0.10	N.D.	N.D.	N.D.	N.D.	N.D.	N.D.	N.D.	N.D.	N.D.	N.D.	0004Q09	N.D.
0004T09	0.07	N.D.	N.D.	0.02	0.01	0.14	0.04	0.05	N.D.	N.D.	N.D.	N.D.	0.2	N.D.	N.D.	N.D.	N.D.	N.D.	0004Q10	N.D.
0004T10	0.04	0.04	N.D.	0.01	N.D.	0.04	0.03	0.15	N.D.	N.D.	0.05	N.D.	0.1	N.D.	N.D.	N.D.	N.D.	N.D.	0004Q11	N.D.
0004T11	0.06	0.04	N.D.	0.01	N.D.	0.10	0.03	0.21	N.D.	N.D.	N.D.	N.D.	N.D.	N.D.	N.D.	N.D.	N.D.	N.D.	0004Q12	N.D.
0004T12	0.08	N.D.	N.D.	0.02	N.D.	0.15	0.02	0.06	N.D.	N.D.	N.D.	N.D.	N.D.	N.D.	N.D.	N.D.	N.D.	N.D.	0004Q13	N.D.
0004T13	0.02	N.D.	N.D.	N.D.	N.D.	0.03	N.D.	0.02	N.D.	N.D.	N.D.	N.D.	N.D.	N.D.	N.D.	N.D.	N.D.	N.D.	0004Q14	N.D.
0004T14	0.03	N.D.	N.D.	0.01	N.D.	0.05	N.D.	0.02	N.D.	N.D.	N.D.	N.D.	N.D.	N.D.	N.D.	N.D.	N.D.	N.D.		
0004T15	0.04	0.05	N.D.	0.01	N.D.	0.05	N.D.	0.11	N.D.	N.D.	0.1	N.D.	N.D.	0.8	N.D.	N.D.	N.D.	N.D.		
0004T16	0.07	0.02	N.D.	0.02	N.D.	0.12	0.02	0.19	N.D.	N.D.	N.D.	N.D.	N.D.	N.D.	N.D.	N.D.	N.D.	N.D.		
0004T17	0.14	0.06	0.02	0.03	0.01	0.18	0.05	0.41	28.3	N.D.	0.2	N.D.	N.D.	N.D.	N.D.	N.D.	N.D.	N.D.		
0004T18	0.03	0.06	N.D.	0.01	N.D.	0.03	0.02	0.21	N.D.	N.D.	0.2	N.D.	N.D.	N.D.	N.D.	0.3	N.D.	0.2		

in $\mu g\,m^{-3}$ | in $ng\,m^{-3}$ | in $\mu gC\,m^{-3}$

Table 5. Same as Table 4 but for the MR01-K02 cruise (May 14 - 28, 2001).

No.	Na^+	NH_4^+	K^+	Mg^{2+}	Ca^{2+}	Cl^-	NO_3^-	$NSS\text{-}SO_4^{2-}$	Al	Fe	NC-V	NC-Cr	NC-Ni	NC-Cu	NC-Zn	NC-As	NC-Cd	NC-Pb	No.	EC
0102T01	1.84	3.13	0.26	0.54	1.56	2.11	16.35	10.41	175.9	82.8	6.4	6.4	5.3	2.1	24.0	1.4	0.5	16.6	0102Q01	1.55
0102T02	0.54	1.90	0.11	0.21	0.64	0.66	5.82	9.07	90.3	62.6	1.4	1.9	1.5	2.3	18.7	1.1	0.4	12.6	0102Q02	0.73
0102T03	0.15	0.65	0.13	0.09	0.20	0.23	1.32	2.41	61.5	40.7	0.4	N.D.	0.5	N.D.	6.6	0.5	0.1	3.8	0102Q03	0.45
0102T04	0.51	0.10	0.22	N.D.	0.16	0.86	0.34	0.41	12.9	5.8	0.1	N.D.	0.5	N.D.	N.D.	N.D.	N.D.	0.3	0102Q04	0.44
0102T05	0.26	0.72	0.06	N.D.	N.D.	0.21	0.13	2.60	128.0	78.4	0.3	N.D.	0.5	N.D.	6.8	0.6	0.2	4.9	0102Q05	0.61
0102T06	0.13	0.26	0.04	0.07	0.19	0.21	1.30	1.15	85.4	54.1	0.2	0.8	0.5	N.D.	6.0	0.3	0.1	2.8	0102Q06	0.23
0102T07	0.10	0.87	0.05	0.08	0.12	0.04	0.47	2.34	145.1	52.2	0.3	N.D.	0.3	N.D.	4.3	0.5	0.1	3.4	0102Q07	0.08
0102T08	0.12	0.56	0.04	0.10	0.15	0.14	0.38	1.49	57.6	24.2	0.2	N.D.	0.1	N.D.	3.0	0.3	0.1	2.3	0102Q08	0.35
0102T09	0.12	0.06	N.D.	N.D.	N.D.	0.31	0.21	0.28	N.D.	N.D.	0.2	N.D.	N.D.	N.D.	N.D.	N.D.	N.D.	0.3	0102Q09	0.45
0102T10	0.45	0.44	0.20	N.D.	0.16	0.50	N.D.	1.75	59.8	12.6	0.5	N.D.	0.3	N.D.	3.1	0.3	0.1	2.0		
0102T11	0.17	0.62	0.16	N.D.	N.D.	0.17	0.14	2.15	34.2	13.6	0.5	N.D.	0.4	N.D.	3.1	0.2	N.D.	2.2		
0102T12	0.22	1.90	0.16	N.D.	N.D.	0.19	0.20	5.14	93.4	53.8	1.1	N.D.	0.5	2.0	14.4	1.0	0.3	9.4		
0102T13	0.03	0.41	N.D.	N.D.	N.D.	N.D.	N.D.	1.53	17.6	N.D.	1.2	N.D.	0.5	N.D.	6.8	0.2	N.D.	1.2		

in $\mu g\,m^{-3}$ | in $ng\,m^{-3}$ | in $\mu gC\,m^{-3}$

3.1.3 Chemical Components and Backward Trajectory

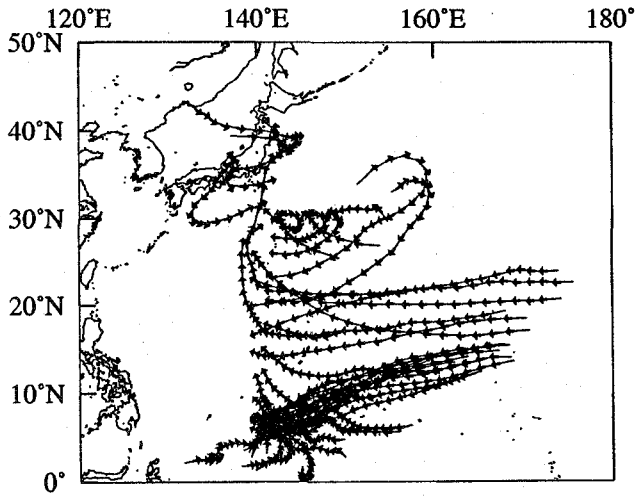

Figure 6. Backward isentropic trajectories for 5 days during the MR00-K04 cruise (21:00 Jun. 13 - 9:00 Jul. 5, 2000).

Figure 5 shows the time series of chemical components of atmospheric aerosols. Figure 5A, 5B, and 5C show concentrations of metal components (NC-V, NC-Ni, and NC-Pb), EC, and ionic components, respectively.

Table 4 also summarizes the concentrations.

There are no sources of metal components and EC over oceans. The V and Ni are indicators of exhaust from heavy oil combustion (Nriagu and Pacyna, 1988); Pb is an indicator of automobile exhaust from leaded gasoline combustion; and EC is an indicator of exhaust from fossil fuel combustion and biomass burning (Seinfeld and Pandis, 1998).

As shown in Fig. 5B, the elemental carbon concentration decreased from 0.21 μ gC m^{-3} to below the detection limit after June 19. Concentrations of metal components such as NC-V, NC-Ni, and NC-Pb in period A were higher than in the period B. They seemed a little affected by anthropogenic sources near Japan. On the other hand, it was found that the air mass was not strongly influenced by anthropogenic emissions in period B.

Over the ocean, the ionic components of aerosols are provided both from anthropogenic and from natural sources. Among natural sources, there are sea-salt particles that are rich in Na^+, Cl^-, SO_4^{2-}, Mg^{2+}, and Ca^{2+}, and dimethylsulfide (DMS) is produced by marine microorganisms.

Oxidation of DMS is a major source of maritime SO_2, which is oxidized to sulfate. Concentrations of atmospheric aerosols also depend on meteorological conditions such as wind speed and precipitation

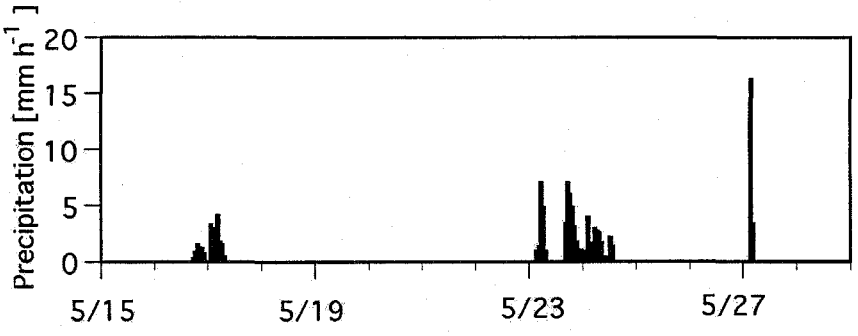

Figure 7. Time series of precipitation during the MR01-K02 cruise (May 15 - 28, 2001).

(Parungo et al., 1986). Concentrations of NSS-SO_4^{2-} in period A were relatively high, 0.51 and 0.37 μ g m^{-3}, and derived from anthropogenic emission as suggested from the concentrations of metal components. Nitrate and ammonium salt are also of anthropogenic origin, and their behavior were similar to that of NSS-SO_4^{2-}. In period B, the concentrations of NSS-SO_4^{2-} ranged from 0.02 - 0.4 μ g m^{-3}, NO_3^-, and NH_4^+ were both less than 0.06 μ g m^{-3}.

Various concentrations of ionic components over the Pacific Ocean have been reported in former investigations. Concentrations of NSS-SO_4^{2-} ranged 0.28 - 0.93 μ g m^{-3} on several islands over the north Pacific Ocean (Savoie et al., 1989). Measurement at Hahajima, a southern island in Japan showed mean concentrations of NSS-SO_4^{2-}, NO_3^- and NH_4^+ of 0.4 μ g m^{-3}, 0.04 μ g m^{-3} and 0.04 μ g m^{-3}, respectively, with particles of less than 2 μ m in diameter (Matsumoto et al., 1998). Parungo et al. (1986) measured at 150° -170° W, 0° -20° N, and the concentrations of NSS-SO_4^{2-}, NO_3^-, and NH_4^+ were 0.17 - 0.45 μ g m^{-3}, 0.06 - 0.13 μ g m^{-3}, and 0.01 - 0.28 μ g m^{-3}, respectively. Huebert et al. (1993) measured at almost the same area, and found that concentration of NSS-SO_4^{2-} particles with diameters less than 1 μ m was 0.19 - 0.67 μ g m^{-3}. Our measured concentrations in period B are in good agreement with this.

Figure 6 shows the backward trajectories for the MR00-K04 cruise calculated every 12hours. Air parcels come from the continent when R/V Mirai cruised along the coast of Japan. On the other hand, south of 30° N, air parcels have a tendency to come from the east or south and pass through to the west or north.

3.2 MR01-K02 Cruise

3.2.1 Optical Properties and Weather Conditions

Figure 7 shows the time series of the precipitation for the MR01-K02 cruise. It rained from 18:00 May 16 to 8:00 May 17 and from 3:00 May 23 to 20:00 May 24 and these periods are expressed as the P periods. Figure 8 presents the time series of the volume scattering coefficient (σ_{sp}), volume absorption coefficient (σ_{ap}), single scattering albedo (ω), and aerosol optical thickness (AOT) at 550nm wavelength. In Fig. 8, period C is 2:00 May 18 to 2:00 May 23, and period D is 22:00 May 24 to 8:00 May 27. The right side of Table 3 lists statistics of σ_{sp}, σ_{ap}, ω, AOT, and α in periods C, D, and P.

When R/V Mirai left Yokosuka, the values of σ_{sp}, σ_{ap}, and ω were 70.9×10^{-6} m^{-1}, 29.3×10^{-6} m^{-1}, and 0.71, respectively, those are values of an urban atmosphere. Figure 8 shows that while R/V Mirai cruised away from the coast until 17 May, the values decreased to relatively clean. Then, under the high pressure system on 18 to 22 May in period C, the values of the optical properties are relatively high as shown in Table 3. The median value of σ_{ap} was 2.17×10^{-6} m^{-1}, which was 20 times higher than that of period B in the MR00-K04 cruise, and ω was 0.85. In period D, 25 - 27 May, σ_{sp} and σ_{ap} returned to the high values of 92.5×10^{-6} m^{-1} and 12.3×10^{-6} m^{-1}, respectively. The value of σ_{sp} is comparable to that in urban atmospheres. During the D period, the median value of AOT was 0.50, 8 times that in period B in the MR00-K04 cruise as shown in Table 3. In periods C and D the aerosol burden was heavy, and that absorptive aerosols were dominant.

For satellite remote sensing, the value of ω is necessary to retrieve AOT. However, as there is little data of ω over the Pacific Ocean, the value of ω has been assumed. As shown in Fig. 8, ω

was not constant but variable from 0.82 to nearly 1.0, and our measured values of ω provide a more accurate estimate of AOT from the remote sensing, and then, more precise evaluation of aerosol

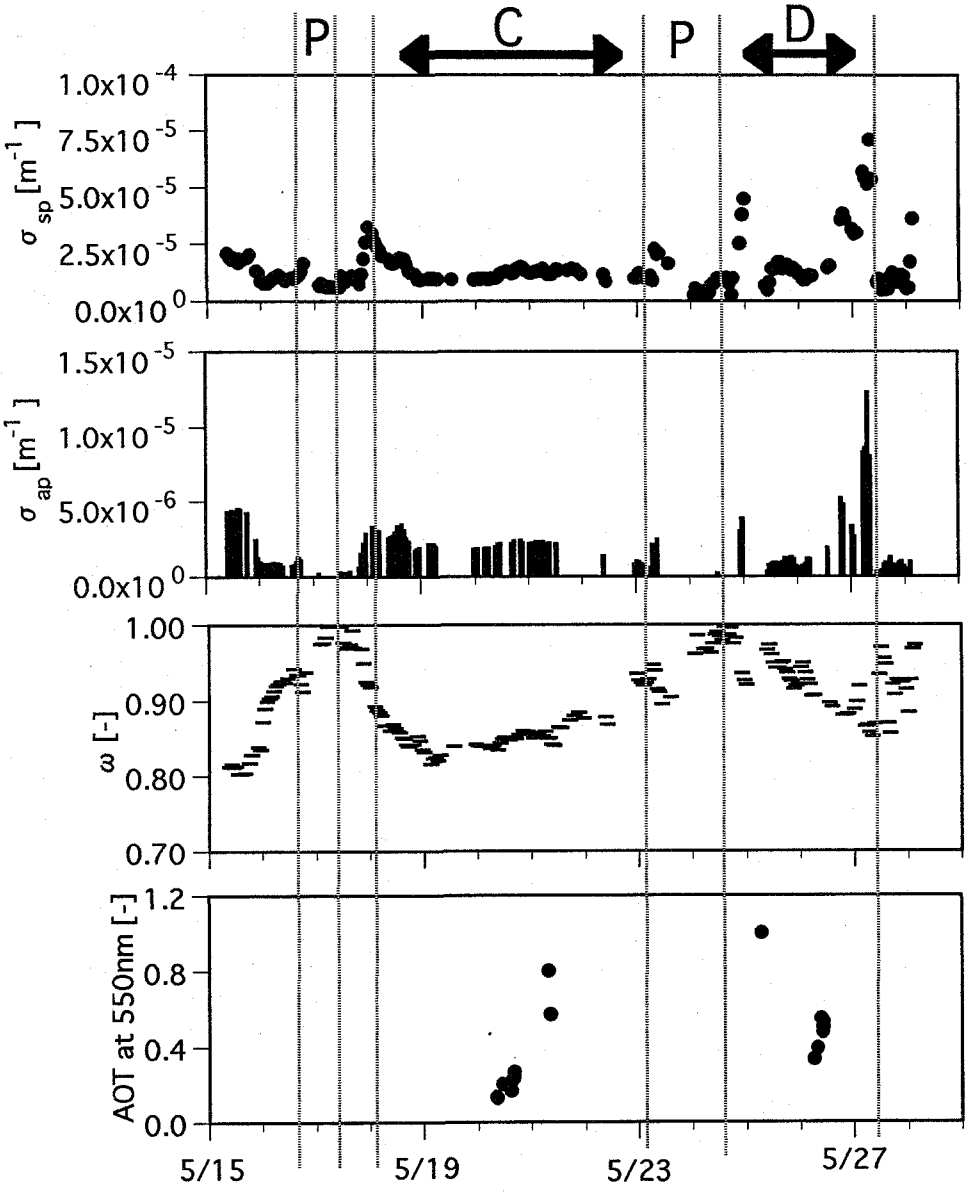

Figure 8. Time series of the volume scattering coefficient (σ_{sp}), volume absorption coefficient (σ_{ap}), single scattering albedo (ω), and aerosol optical thickness (AOT) at 550nm wavelength for the MR01-K02 cruise (May 15 - 28, 2001). Period P is 18:00 May 16 to 8:00 May 17 and 3:00 May 23 to 20:00 May 24. Period C is 2:00 May 18 to 2:00 May 23, and period D is 22:00 May 24 to 8:00 May 27. It was rainy during period P, and there was no precipitation during periods C and D.

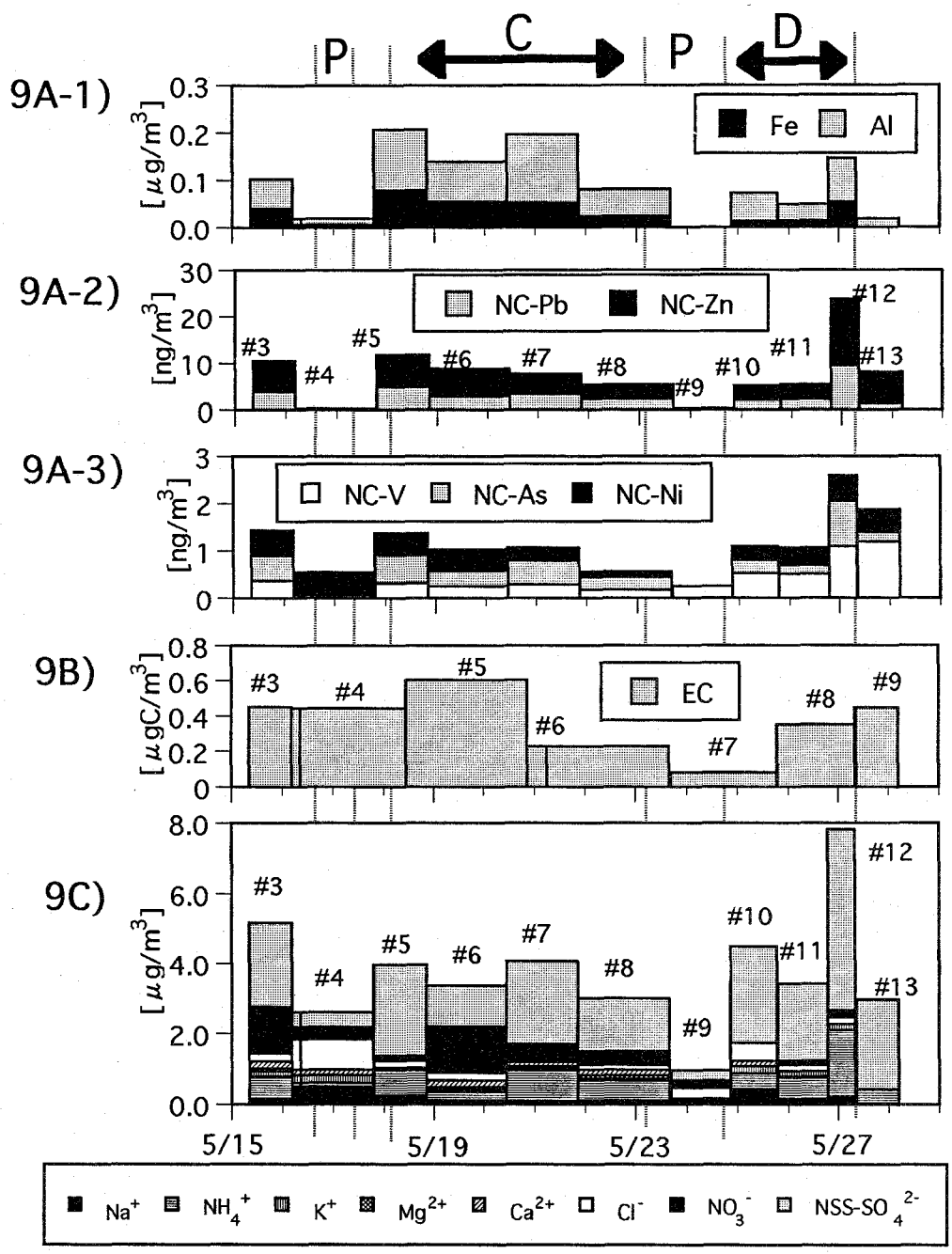

Figure 9. Time series of the concentrations of metal components (Fig. 9A-1 to Fig. 9A-3), elemental carbon (Fig. 9B), and ionic components (Fig. 9C) for the MR01-K02 cruise (May 15 - 28, 2001). #3 - #13 represent filter sample numbers. #3 - #13 in Fig. 9A-2 and 9C and #3 - #9 in Fig. 9B correspond to filter numbers 0102T** and 0102Q** in Tables 2 and 5.

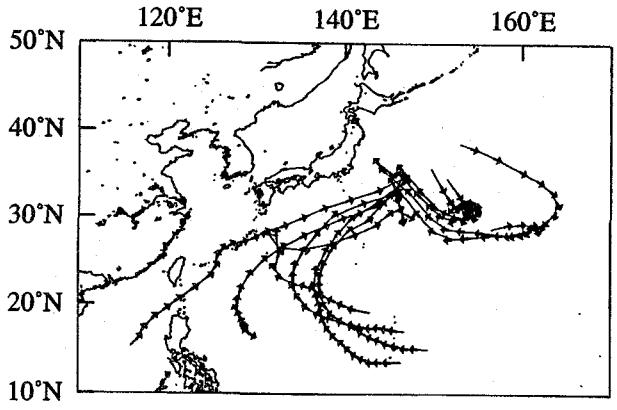

Figure 10. Backward isentropic trajectories for 5 days for the MR01-K02 cruise in period P.

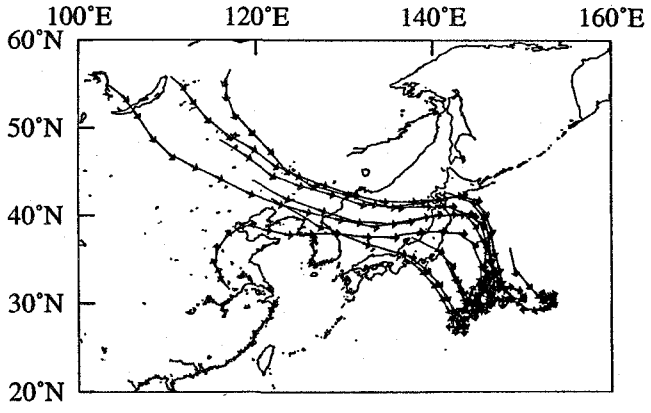

Figure 11. Backward isentropic trajectories in period C for the MR01-K02 cruise.

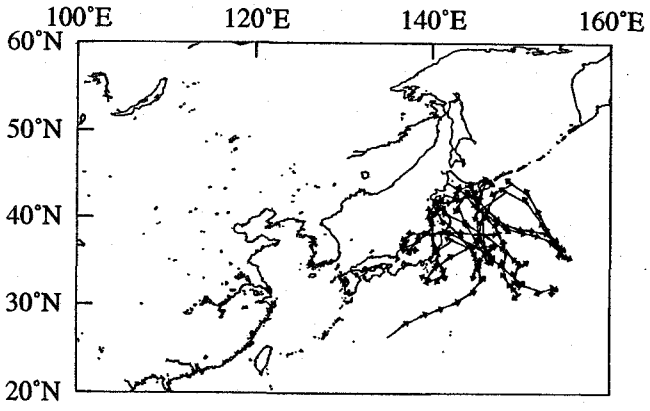

Figure 12. Backward isentropic trajectories in period D for the MR01-K02 cruise.

radiative foring.

3.2.2 Chemical Components and Backward Trajectories

Figures 9A, 9B, and 9C show time series of the concentrations of metal components (Al, Fe, NC-V, NC-Ni, NC-Pb, NC-Zn, and NC-As), EC, and ionic components, respectively. Table 5 summarizes the concentrations of chemical components of atmospheric aerosols.

The period P aerosol samples in Fig. 9 were mainly collected during rain, and concentrations of aerosol chemical species are lower than in the other periods of MR01-K02 and slightly lower than those in period A in the MR00-K04 cruise. Averaged concentrations of NC-V and NSS-SO_4^{2-} in period P were 0.16 ng m^{-3} and 0.35 μ g m^{-3}, respectively. The EC concentration of #0102Q07 was 0.08 μ gC m^{-3}.The low concentrations in these samples result from washout of aerosols, and the inflow of a clean southern air mass due to the passage of a low pressure. Figure 10 shows backward trajectories calculated for every 6 hours for period P. The air flows from the south of Japan in this period.

In periods C and D, samples were mainly collected during non-precipitating periods. In Fig. 9, concentrations of NC-V, NSS-SO_4^{2-}, and NH_4^+ were 0.2 - 1.1 ng m^{-3}, 1.2 - 5.1 μ g m^{-3}, and 0.3 - 1.9 μ g m^{-3}, respectively, 1.3 to 20 times higher than those during period P and on average 15 to 30 times higher than

those of period B in the MR00-K04 cruise. The non crustal Arsenic (NC-As) concentration was 0.5 ng m^{-3} on average which is an indicator of coal combustion (Nriagu and Pacyna, 1988). The averaged EC concentration was 0.4 μ gC m^{-3} which is 5 times higher than that in #0102Q07, and it caused the increased σ_{ap} in Fig. 8. High concentrations of NC-V, NC-Ni, NC-Pb, NC-Zn, NC-As, and EC in periods C and D imply transport of anthropogenic aerosols to 500km off from the coast. During these periods, Al and Fe were also detected, and they represent indicators of soil particles. Average concentrations of Al was 86ng m^{-3} and of Fe 41ng m^{-3}. The average ratio of Fe over Al was 0.48, which is close to the 0.44 of crustal rock (Seinfeld and Pandis, 1998). Thus, during these periods, not only anthropogenic aerosols, but also soil particles may be assumed to have been transported. Figures 11 and 12 show backward trajectories calculated every 12 hours in period C and every 6 hours in period D. Air parcels tend to come from the continent in period C (Fig. 11) and from Japan in period D (Fig. 12).

4. Conclusion

South of 30° N during the MR00-K04 cruise in June-July, 2000 was covered with a maritime air mass. The median value of σ_{sp} was 12.8×10^{-6} m^{-1}, σ_{ap} was 0.1×10^{-6} m^{-1}, and ω was 0.99. Concentrations of NSS-SO_4^{2-} were from 0.02 - 0.4 μ g m^{-3}, and NO_3^- and NH_4^+ were below 0.06 μ g m^{-3}. The EC values were lower than the detectable limit. In the marine environment sea salt particles are dominant, and anthropogenic sources are not so strongly represented. Then, when anthropogenic aerosols invade from land over ocean, the typical maritime conditions are drastically perturbed. During the non-precipitation period of the MR01-K02 cruise, anthropogenic aerosols and soil particles were detected 500km off the coast. The median value of σ_{ap} was 2.17×10^{-6} m^{-1}, 20 times higher than that in the maritime air mass. Here the median value of ω was 0.85, 14% down, and AOT was 0.50, 8 times higher. The values of ω were not constant but varied from 0.82 to nearly 1.0. Anthropogenic aerosol components NSS-SO_4^{2-}, NO_3^-, and NH_4^+ were 10 to 20 times higher than those south of 30° N measured in the MR00-K04 cruise. The averaged EC concentration was 0.4 μ gC m^{-3} which caused the increase in σ_{ap}.

To estimate the aerosol direct forcing, both the spatial distribution of aerosol burden and the frequency of invasion must be known. Satellite remote sensing is available to determine these parameters. Further, there is a need to accumulate more *In-situ* data of optical and chemical properties of aerosols in various air conditions.

Acknowledgments

This study was conducted at the MR00-K04 and MR01-K02 cruises of R/V Mirai. We wish to express thanks to the Japan Marine Science and Technology Center, and also to Dr. MIURA Kazuhiko (Science University of Tokyo) for his support in the cruises.

References

Anderson T.L., Covert D.S., Wheeler J.D., Harris J.M., Perry K.D., Trost B.E., Jaffe D.J., and Ogren

J.A. (1999): Aerosol backscatter fraction and single scattering albedo: Measured values and uncertainties at a coastal station in the Pacific Northwest. J. Geophys. Res., 104, pp. 26793-26807

Bodhaine B.A. (1995): Aerosol absorption measurements at Barrow, Mauna Loa and the south pole. J. Geophys. Res., 100, pp.8967-8975

Bond T.C., Anderson T. L., and Campbell D., (1999): Calibration and Intercomparison of Filter-Based Measurements of Visible Light Absorption by Aerosol, Aerosol Sci. and Tech., 30, pp.582-600

Charlson R.J., Schwartz S.E., Hales J.M., Cess R.D., Coakley J.A., Jr., Hansen J.E., and Hofmann D.J. (1992): Climate forcing by anthologenic aerosols. Science, 255, pp.423-430

Huebert B.J., Howell S., Laj P., Johnson J.E., Bates T.S., Quinn P.K., Yegorov V., Clarke A.D., and Porter J.N. (1993): Observations of the atmospheric sulfur cycle on SAGA3. J. Geophys. Res., 98, pp.16985-16995

IPCC 1996 (1996): Climate change 1995, The Science of Climate Change, Cambridge University Press

Matsumoto K., Nagao I., Tanaka H., Miyaji H., Iida T., and Ikebe Y. (1998): Seasonal characteristics of organic and inorganic species and their size distributions in atmospheric aerosols over the northwest pacific ocean. Atmos. Environ., 32, pp.1931-1946

Nakajima T., Tonna G., Rao R., Boi P., Kaufman Y., and Holben B. (1996): Use of sky brightness measurements from ground for remote sensing of particulate polydispersions, Applied Optics, 35, pp. 2672-2686

Nakajima T., Higurashi A., Aoki K., Endoh T., Fukushima H., Member, IEEE, Toratani M., Mitomi Y., Mitchell B.G., and Frouin R. (1999): Early phase analysis of OCTS radiance data for aerosol remote sensing. IEEE Transactions on geoscience and remote sensing, 37, pp.1575-1585

Nriagu J.O. and Pacyna J.M. (1988): Quantitative assessment of worldwide contamination of air, water and soils by trace metals. Nature, 333, pp.134-139

Ohta S. and Okita T. (1984): Measurements of particulate carbon in urban and marine air in Japanese areas. Atmos. Environ., 18, pp.2439-2445

Parungo F.P., Nagamoto C.T., Rosinski J., and Haagenson P.L. (1986): A study of marine aerosols over the Pacific Ocean. J. Atmos. Chem., 4, pp.199-226

Savoie D.L., Prospero J.M., and Saltzman E.S. (1989): Nitrate, non-seasalt sulfate and methanesulfonate over the Pacific Ocean. Chem. oceanography, 10, pp.219-250

Seinfeld J.H. and Pandis S.N. (1998): Atmospheric chemistry and physics. John Wiley & Sons